Convection in Rotating Spherical Fluid Shells

F. H. Busse* and R. Simitev

Institute of Physics, University of Bayreuth, D-95440 Bayreuth, Germany

"Mathematical Aspects of Natural Dynamos", E. Dormy, A.M. Soward (eds.), Grenoble Sciences and CRC Press, Boca Raton, pp. 119-198, ISBN-13:978-1-58488-954-0, 2007.

1 Introduction

Convection driven by thermal buoyancy in rotating spherical bodies of fluid has long been recognized as a fundamental process in the understanding of the properties of planets and stars. Since these objects are rotating in general and since their evolution is associated with the transport of heat from their interiors convection influenced by the Coriolis force does indeed play a dominant role in the dynamics of their fluid parts. In the case of the Earth it is the generation of the geomagnetic field by motions in the molten outer iron core which has stimulated much interest in the subject of convection in rotating spheres. But the zones and belts seen on Jupiter are a just as interesting phenomenon driven by convection in the deep atmosphere of the planet. Similarly, the differential rotation of the sun and its magnetic cycle are intimately connected with the solar convection zone encompassing the outer 29 percent of the Sun in terms of its radial extent.

Theoretical studies of convection in rotating fluid spheres started about 50 years ago. The attention was restricted to the linear problem of the onset of convection and for simplicity axisymmetric motions were assumed. An account of these early efforts can be found in Chandrasekhar's famous treatise (1961) and in the papers by Bisshopp and Niiler (1965) and by Roberts

*e-mail: Busse@uni-bayreuth.de

(1965). A little later it became evident that the preferred forms of convection in the interesting limit of rapid rotation are not axisymmetric, but highly non-axisymmetric (Roberts, 1968). In this later paper, however, the incorrect assumption was made that the preferred mode of convection exhibits a z-component of the velocity field parallel to the axis that is symmetric with respect to the equatorial plane. The correct mode for the onset of convection was found by Busse (1970a) who approached the problem on the basis of the rotating cylindrical annulus model. This model takes advantage of the approximate validity of the Proudman-Taylor theorem and the analysis can thus be reduced from three to two spatial dimensions. We shall devote section 2 to a description of this model since it offers the simplest access to the spherical problem.The basic equations for the spherical problem are introduced in section 3 and the onset of columnar convection in spherical shells is discussed in section 4. In section 5 the onset of inertial mode convection is described which prevails at very low Prandtl numbers. In section 6 the properties of finite amplitude convection are outlined for moderately low Prandtl numbers Pr, while convection at higher values of Pr is considered in section 7. In section 8 equatorially attached convection is considered which evolves from inertial mode convection. The problem of penetrative convection is addressed in section 9 and in section 10 some aspects of convection in the presence of thermal as well as chemical buoyancy are discussed. The chapter concludes with some remarks on applications among which the dynamo action of convection is of special importance.

2 Convection in the Rotating Cylindrical Annulus

Convection in the fluid filled gap between two rigidly rotating coaxial cylinders is receiving increasing attention because it shares many linear and nonlinear dynamical properties with convection in rotating spherical fluid shells, at least as far as columnar convection is concerned. From the point of view of planetary applications it seems natural to have gravity pointing inward and to keep the inner cylinder at the higher temperature T_2. But since the centrifugal force is used as a source of buoyancy in laboratory experiments with the higher temperature at the outer cylinder we shall use this latter configuration as shown in Fig. 1. Since only the product of effective gravity and applied temperature gradient is physically relevant the two cases are equivalent. In experimental realizations of the system ordinary gravity plays a minimal role when a

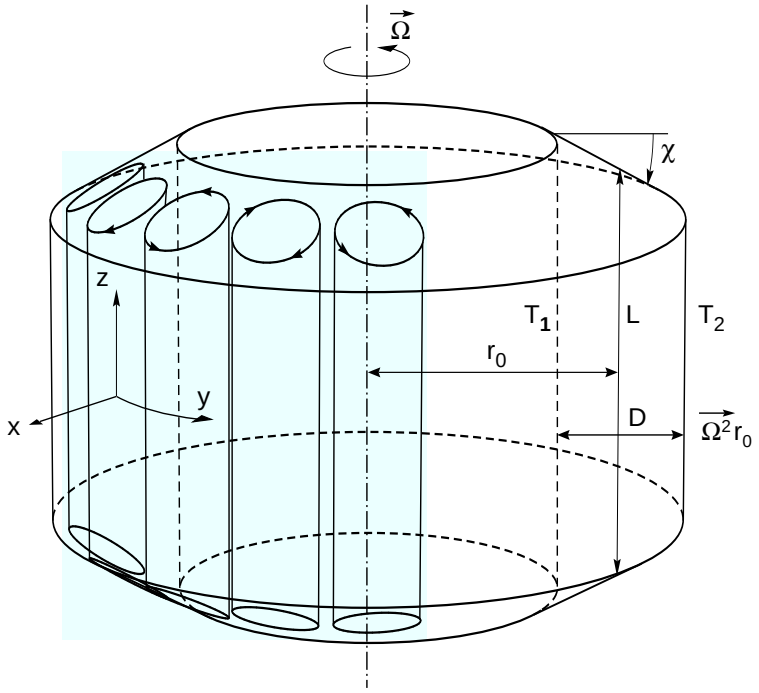

Figure 1: *Sketch of the geometrical configuration of the rotating cylindrical annulus.*

vertical axis of rotation is used and when the rate of rotation is sufficiently high such that the centrifugal force exceeds gravity by at least a factor of two or three. An important ingredient of the geometrical configuration shown in Fig. 1 are the conical boundaries at top and bottom which cause a variation in height with distance from the axis of rotation. Without this variation in height steady two-dimensional convection rolls aligned with the axis will be realized since they obey the Proudman-Taylor condition. The Coriolis force is entirely balanced by the pressure gradient in this case and Rayleigh number for onset of convection in the small gap limit is given by the Rayleigh-Bénard value for a non-rotating layer. Thin Ekman layers at the no-slip top and bottom boundaries exert only a minor influence on the dynamics of convection if the height L of the annulus is sufficiently large in comparison to the gap size. As soon as the height changes in the radial direction any flow involving a radial velocity component can no longer satisfy the geostrophic balance. Instead a weak time dependence is required and the flow assumes the character of Rossby waves.These waves are well known in the meteorological context

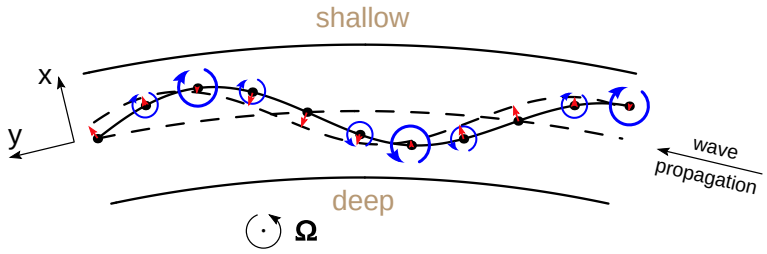

Figure 2: *The mechanism of propagation of a Rossby wave visualized in the equatorial plane of the rotating annulus: Fluid columns originally resting at the mid-surface acquire anti-cyclonic vorticity relative to the rotating system when they are displaced outwards towards the shallow region. Cyclonic vorticity is acquired by the columns displaced inwards. The action of the columnar motion on the neighboring fluid columns is such that an initial sinusoidal displacement propagates in the prograde direction.*

where the variation of the vertical component of rotation with latitude has the same effect as variation of height in the annulus of Fig. 1. The dynamics of Rossby waves can be visualized most readily if the action of the vorticity acquired by the fluid columns displaced radially from the middle of the gap is considered. As indicated in Fig. 2 columns shifted inward acquire cyclonic vorticity because they are stretched owing to the increasing height. The opposite sign of vorticity is exhibited by columns moving outward. Since their moments of inertia are increased they must rotate anti-cyclonically relative to the rotating system in order to conserve angular momentum. The action of the acquired motion of sinusoidally displaced columns on their neighbors results in the propagation of a wave as shown in Fig. 2. The phase velocity is in the prograde (retrograde) direction hen the height decreases (increases) with distance from the axis.

In the case of convection the dynamics is modified by the presence of thermal buoyancy and the phase velocity is less than that of Rossby waves except in the limit of vanishing Prandtl number. The analysis of the thermal Rossby waves, as the propagating convection waves are called, is quite simple if the inclination of the cones with respect to the equatorial plane is introduced as a small perturbation. Using the gap width D as length scale and D^2/ν as time scale where ν is the kinematic viscosity of the fluid we may assume the velocity field in the form

$$\mathbf{u} = \nabla\psi(x, y, t) \times \mathbf{k} + \dots \tag{1}$$

where $\mathbf{k}$ is the unit vector in the z-direction parallel to the axis of rotation and where the small gap approximation with x as radial coordinate and y as azimuthal coordinate has been assumed. Only the geostrophic component of $\mathbf{u}$ has been denoted explicitly in expression (1). Deviations from geostrophy are induced by the condition of vanishing normal velocity at the conical boundaries,

$$u_x\eta_0 \pm u_z = 0 \quad \text{at} \quad z = \pm\frac{L}{2D} \tag{2}$$

where the tangent η_0 of the angle χ between the cones and the equatorial plane has been introduced as small parameter. By taking the z-component of the curl of the equation of motion and averaging it over the height of the annulus we can incorporate the boundary condition (2) into an equation for $-\Delta_2\psi$ which is the z-component of vorticity,

$$\left(\frac{\partial}{\partial t} + \frac{\partial}{\partial y}\psi\frac{\partial}{\partial x} - \frac{\partial}{\partial x}\psi\frac{\partial}{\partial y}\right)\Delta_2\psi - \Delta_2^2\psi - \eta\frac{\partial}{\partial y}\psi = -\frac{\partial}{\partial y}\Theta \tag{3}$$

where Δ_2 is the two-dimensional Laplacian, $\Delta_2 = \partial^2/\partial x^2 + \partial^2/\partial y^2$. Equation (3) must be considered together with the heat equation for the deviation Θ from the static temperature distribution of pure conduction,

$$Pr\left(\frac{\partial}{\partial t} + \frac{\partial}{\partial y}\psi\frac{\partial}{\partial x} - \frac{\partial}{\partial x}\psi\frac{\partial}{\partial y}\right)\Theta + \frac{\partial}{\partial y}\psi = \Delta_2\Theta. \tag{4}$$

where Θ is measured in multiples of $(T_2 - T_1)Pr/Ra$. T_1 and T_2 are the temperatures prescribed at the inner and outer cylindrical boundaries, respectively. The dimensionless Coriolis parameter η, the Rayleigh number Ra and the Prandtl number Pr are defined by

$$\eta = \frac{4\Omega\eta_0 D^3}{\nu L}, \quad Ra = \frac{\gamma(T_2 - T_1)\Omega^2 r_0 D^3}{\nu\kappa}, \quad Pr = \frac{\nu}{\kappa}.$$

where Ω denotes the angular velocity of rotation, γ is the coefficient of thermal expansion, κ is the thermal diffusivity and r_0 is the mean radius of the annulus. Assuming stress-free boundaries at the cylindrical walls,

$$\psi = \frac{\partial^2}{\partial x^2}\psi = \Theta = 0 \quad \text{at} \quad x = \pm\frac{1}{2}, \tag{5}$$

we obtain a completely specified mathematical formulation of the problem of centrifugally driven convection in the cylindrical annulus.

The onset of convection is described by the linearized version of Eqs. (3) which can be solved by

$$\psi = A \sin n\pi(x+\frac{1}{2}) \exp\{i\alpha y + i\omega t),$$
$$\Theta = \frac{-i\alpha\psi}{\alpha^2 + (n\pi)^2 + i\omega}, \tag{6}$$

with the following relationships for ω and Ra

$$\omega = \frac{-\eta\alpha}{(1+Pr)(n^2\pi^2+\alpha^2)},$$
$$Ra = (n^2\pi^2+\alpha^2)^3\alpha^{-2} + \left(\frac{\eta Pr}{1+Pr}\right)^2 (n^2\pi^2+\alpha^2)^{-1}. \tag{7}$$

As expected the dependence of Rayleigh number on the wavenumber in the case of Rayleigh-Bénard convection in a non-rotating layer is recovered in the limit $\eta = 0$. The mode corresponding to $n = 1$ is preferred in this case, of course. This property continues to hold for finite η. But as the limit $\eta \to \infty$ is approached, the values of Ra and ω do not depend on n in first approximation as can be seen from the following expressions for the critical values in the limit of large η

$$\alpha_c = \eta_P^{\frac{1}{3}}(1 - \frac{7}{12}\pi^2\eta_P^{-\frac{2}{3}} + \ldots)$$
$$Ra_c = \eta_P^{\frac{4}{3}}(3 + \pi^2\eta_P^{-\frac{2}{3}} + \ldots)$$
$$\omega_c = -\sqrt{2}Pr^{-1}\eta_P^{\frac{2}{3}}(1 - \frac{5}{12}\pi^2\eta_P^{-\frac{2}{3}} + \ldots) \tag{8}$$

where the definition $\eta_P = \eta Pr\sqrt{1/2}(1+Pr)^{-1}$ has been used. Expressions (8) have been derived for $n = 1$, but they hold for arbitrary n when π^2 is replaced by $(n\pi)^2$ The weak dependence on the radial coordinate of the problem has two important consequences:

(i) The onset of convection is rather insensitive to the cylindrical boundaries. The analysis can thus be applied to the case of a sphere where these boundaries are missing.

(ii) Modes of different radial dependence correspond to the same critical parameters asymptotically. Secondary bifurcations right above threshold become possible through couplings of these modes.

The latter possibility is indeed realized in the form of the mean flow instability. A transition to a solution of the form

$$\psi = A\sin(\alpha y - \omega t)\sin\pi(x+\frac{1}{2}) + B\sin(\alpha y - \omega t + \varphi)\sin 2\pi(x+\frac{1}{2}) \qquad (9)$$

occurs as the Rayleigh number is increased beyond the critical value unless the Prandtl number is rather small (Or and Busse, 1987). A characteristic property of solution (9) is the strong mean zonal shear which it generates through its Reynolds stress, $\overline{u_x u_y} \propto AB\sin\pi(x+\frac{1}{2})\sin\varphi$, where the bar indicates the average over the y-coordinate. Both signs of the shear are equally possible since the sign of B is arbitrary. The mean flow instability corresponds to a tilt of the convection columns as indicated in Fig. 3. When the columns are slightly tilted in the prograde sense towards the outside prograde momentum is carried outward and retrograde momentum is transported inwards leading to a differential rotation in which the outer fluid rotates faster than the inner one. An equilibrium is reached through viscous stresses which tend to oppose the differential rotation. The reverse situation occurs when the columns are tilted the other way as shown in the right plot of Fig. 3. The instability occurs because the differential rotation tends to increase the initial tilt and a feedback process is thus initiated. The mean flow instability of convection rolls is also possible in a non-rotating Rayleigh-Bénard layer. But there it is usually preceded by three-dimensional instabilities.

There is another way in which a differential rotation in the annulus can be generated. When curved cones instead of straight cones are used as indicated in Fig. 4 solutions of the form (5) with separating x- and y-dependences are no longer possible. The term $\eta\partial_y\psi$ in Eq. (3a) must now be replaced by $\eta(1+\epsilon x)\partial_y\psi$ where positive ϵ refers to the convex case of Fig. 4 while a negative ϵ corresponds to the concave cones of the right plot. The columns are tilted because the thermal Rossby wave has the tendency to propagate faster on the outside than on the inside when ϵ is positive and vice versa. A differential rotation prograde on the outside and retrograde on the inside must thus be expected for $\epsilon > 0$ as shown in the left plot of Fig. 4 while the opposite results is obtained for $\epsilon < 0$. The experiment of Busse and Hood (1982) has demonstrated this effect.

There are numerous other interesting features of convection in the cylindrical annulus such as vacillations and relaxation oscillations which appear at higher Rayleigh numbers and which can be related to analogous phenomena of convection in rotating spheres. We refer to the papers by Or and Busse (1987), Schnaubelt and Busse (1992), Brummell and Hart (1993) for details.

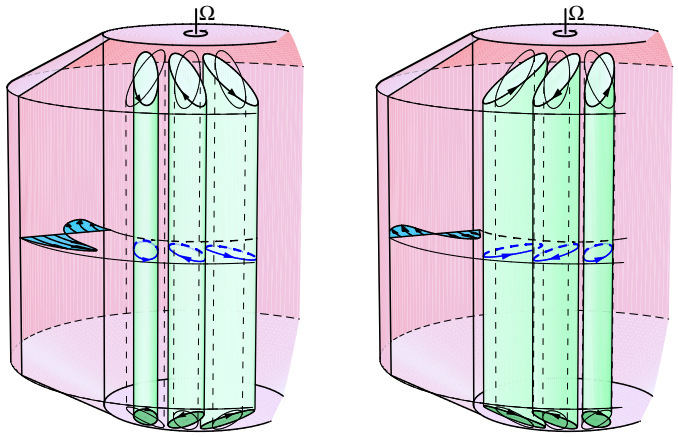

Figure 3: *The mean flow instability leading to either outward (right figure) or inward (left figure) transport of prograde angular momentum.*

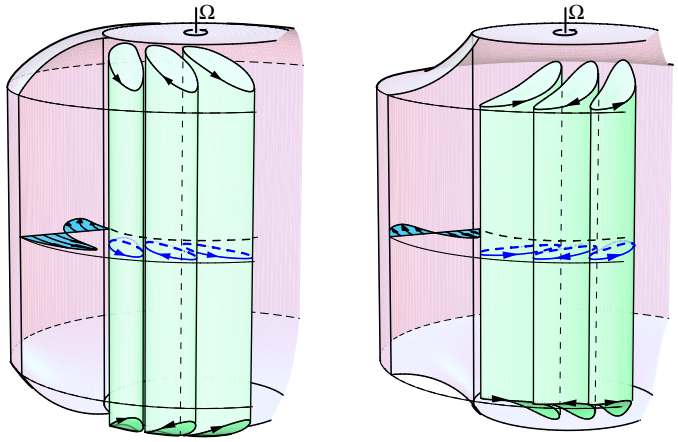

Figure 4: *Influence of curved conical boundaries. In the convex case (right figure) the columns tend to spiral outward in the prograde direction. They thus create a different rotation with higher angular velocity on the outside than on the inside. The opposite situation is found in the concave case (left figure).*

The influence of non-axisymmetric modulations of the boundaries can also easily be investigated in the annulus model as shown by Bell and Soward (1996), Herrmann and Busse (1997) and Westerburg and Busse (2003). Besides the narrow gap limit the finite gap case of the rotating cylindrical annulus system is also of interest. The discrete manifold of realizable wavenumbers gives rise to resonances and changes in the character of secondary instabilities. We refer to the recent papers by Pino *et al.* (2000, 2001) and Chen and Zhang (2002).

3 Mathematical Formulation of the Problem of Convection in Rotating Spherical Shells

The presence of the centrifugal force in rotating planets and stars usually causes some deviations from spherical symmetry. The surfaces of constant potential become spheroidal and a basic state of vanishing motion relative to a rotating frame of reference may not exist since surfaces of constant density do not coincide with surfaces of constant potential in general. As a result of this baroclinicity a differential rotation must be expected (see, for example, Busse, 1982). But these effects are usually much smaller than those introduced by convection and it is thus a good approximation to neglect the effects of the centrifugal force and to assume that there exists a basic static solution with spherically symmetric distributions of gravity and temperature.

For the theoretical description of thermal convection in rotating spheres usually the case of a gravity varying linearly with radius, $\mathbf{g} = -g_0 d\mathbf{r}$ is assumed where $\mathbf{r}$ is the position vector with respect to the center of the sphere which is made dimensionless with the thickness d of the shell. We assume that a static state exists with the temperature distribution $T_S = T_0 - \beta d^2 r^2/2 + \Delta T \eta r^{-1}(1-\eta)^{-2}$ where η denotes the ratio of inner to outer radius of the shell and β is proportional to a uniform density of heat sources in the sphere. In addition an applied temperature difference is admitted such that ΔT is the temperature difference between the boundaries in the special case $\beta = 0$. Of course, in geophysical and astrophysical applications only the super-adiabatic part of the temperature field must be identified with the temperature distribution given above.

In addition to d, the time d^2/ν and the temperature $\nu^2/g_0\gamma d^4$ are used as scales for the dimensionless description of the problem where ν denotes the kinematic viscosity of the fluid and κ its thermal diffusivity. We use the Boussinesq approximation in that we assume the density ρ to be constant except in the gravity term where its temperature dependence given by $\gamma \equiv$

$(d\varrho/dT)/\varrho = \text{const.}$ is taken into account. The basic equations of motion and the heat equation for the deviation Θ from the static temperature distribution are thus given by

$$\partial_t \boldsymbol{u} + \boldsymbol{u}\cdot\nabla\boldsymbol{u} + \tau\boldsymbol{k}\times\boldsymbol{u} = -\nabla\pi + \Theta\boldsymbol{r} + \nabla^2\boldsymbol{u} \tag{10a}$$

$$\nabla\cdot\boldsymbol{u} = 0 \tag{10b}$$

$$Pr(\partial_t\Theta + \boldsymbol{u}\cdot\nabla\Theta) = (Ra_i + Ra_e\eta r^{-3}(1-\eta)^{-2})\boldsymbol{r}\cdot\boldsymbol{u} + \nabla^2\Theta \tag{10c}$$

where the Rayleigh numbers Ra_i and Ra_e, the Coriolis number τ and the Prandtl number Pr are defined by

$$Ra_i = \frac{\gamma g_0 \beta d^6}{\nu\kappa},\quad Ra_e = \frac{\gamma g_0 \Delta T d^4}{\nu\kappa},\quad \tau = \frac{2\Omega d^2}{\nu},\quad Pr = \frac{\nu}{\kappa}.$$

Since the velocity field $\boldsymbol{u}$ is solenoidal the general representation in terms of poloidal and toroidal components can be used,

$$\boldsymbol{u} = \nabla\times(\nabla v\times\boldsymbol{r}) + \nabla w\times\boldsymbol{r}.$$

By multiplying the $(\text{curl})^2$ and the curl of equation (10a) by $\boldsymbol{r}$ we obtain two equations for v and w,

$$[(\nabla^2 - \partial_t)L_2 + \tau\partial_\phi]\nabla^2 v + \tau Q w - L_2\Theta = -\boldsymbol{r}\cdot\nabla\times[\nabla\times(\boldsymbol{u}\cdot\nabla\boldsymbol{u})] \tag{11a}$$

$$[(\nabla^2 - \partial_t)L_2 + \tau\partial_\phi]w - \tau Q v = \boldsymbol{r}\cdot\nabla\times(\boldsymbol{u}\cdot\nabla\boldsymbol{u}), \tag{11b}$$

where ∂_t and ∂_ϕ denote the partial derivatives with respect to time t and with respect to the angle ϕ of a spherical system of coordinates r, θ, ϕ and where the operators L_2 and Q are defined by

$$L_2 \equiv -r^2\nabla^2 + \partial_r(r^2\partial_r) \tag{12a}$$

$$Q \equiv r\cos\theta\nabla^2 - (L_2 + r\partial_r)(\cos\theta\partial_r - r^{-1}\sin\theta\partial_\theta). \tag{12b}$$

Stress-free boundaries with fixed temperatures are most often assumed,

$$v = \partial_{rr}^2 v = \partial_r(w/r) = \Theta = 0 \tag{13}$$
$$\text{at}\quad r = r_i \equiv \eta/(1-\eta)\quad\text{and}\quad r = r_o = (1-\eta)^{-1}.$$

The numerical integration of equations (2) together with boundary conditions (4) in the general nonlinear case proceeds with the pseudo-spectral method as described by Tilgner and Busse (1997) which is based on an expansion of all dependent variables in spherical harmonics for the θ, ϕ-dependences, i.e.

$$v = \sum_{l,m} V_l^m(r,t) P_l^m(\cos\theta)\exp\{im\phi\} \tag{14}$$

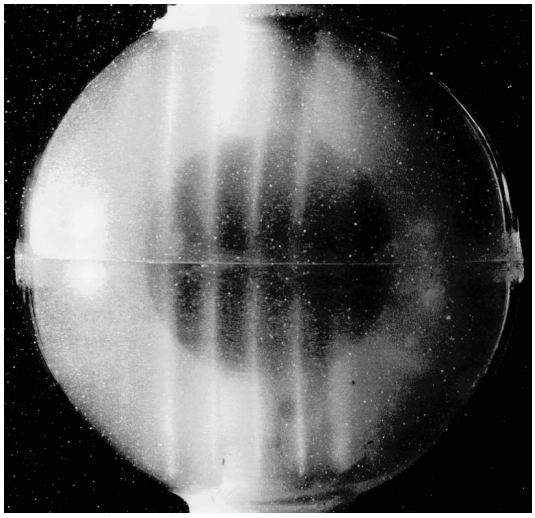

Figure 5: *Centrifugally driven convection in a rotating fluid between an inner cooled and an outer heated spherical boundary. The motions are visualized through nearly neutrally buoyant thin platelets which align themselves with the shear. The photograph shows the onset of thermal Rossby waves in the form of convection columns in a thick fluid shell.*

and analogous expressions for the other variables, w and Θ. P_l^m denotes the associated Legendre functions. For the r-dependence expansions in Chebychev polynomials are used. For further details see also Busse *et al.* (1998). For the computations to be reported in sections 5 and 6 a minimum of 33 collocation points in the radial direction and spherical harmonics up to the order 64 have been used. But in many cases the resolution was increased to 49 collocation points and spherical harmonics up to the order 96 or 128.

4 The Onset of Convection in Rotating Spherical Shells

The main difficulty in analyzing convection in rotating spherical shells arises from the fact that the role of the Coriolis force varies with the angle between gravity and the vector $\mathbf{\Omega}$ of angular velocity. The geometrical configuration of the polar regions of the shell thus resembles that of a Rayleigh-Bénard layer rotating about a vertical axis while in the equatorial region the model of the rotating cylindrical annulus can be applied. Only at low rotation rates does

convection set in in a global fashion and an axisymmetric mode can become preferred in this case (Geiger and Busse, 1981). At higher rotation rates the onset of convection does indeed occur in the form of the columnar modes as predicted on the basis of the annulus model of section 2. A visualisation of the convection motion in the form of thermal Rossby waves traveling in the prograde direction is shown in Fig. 5.

A rough idea of the dependence of the critical Rayleigh number Ra_{ic} for the onset of convection on the parameters of the problem in the case $Ra_e = 0$ can be gained from the applications of expressions (8) of the annulus model,

$$Ra_{ic} = 3\left(\frac{Pr\tau}{1+Pr}\right)^{\frac{4}{3}} (\tan\theta_m)^{\frac{8}{3}} r_m^{-\frac{1}{3}} 2^{-\frac{2}{3}} \tag{15a}$$

$$m_c = \left(\frac{Pr\tau}{1+Pr}\right)^{\frac{1}{3}} (r_m \tan\theta_m)^{\frac{2}{3}} 2^{-\frac{1}{6}} \tag{15b}$$

$$\omega_c = \left(\frac{\tau^2}{(1+Pr)^2 Pr}\right)^{\frac{1}{3}} 2^{-\frac{5}{6}} (\tan^2\theta_m / r_m)^{\frac{2}{3}}, \tag{15c}$$

where r_m refers to the mean radius of the fluid shell, $r_m = (r_i + r_o)/2$, and θ_m to the corresponding colatitude, $\theta_m = \arcsin(r_m(1-\eta))$. The azimuthal wavenumber of the preferred mode is denoted by m_c and the corresponding angular velocity of the drift of the convection columns in the prograde direction is given by ω_c/m_c. In figure 6 the expressions (15a,c) are compared with accurate numerical values in the case $Ra_e = 0$ which indicate that the general trend is well represented by expressions (15a,c). The same property holds for m_c. In the case $Ra_i = 0$ the agreement with expressions (15a,c) is not quite as good since the onset of convection is more concentrated towards the tangent cylinder touching the inner boundary at its equator because of the higher temperature gradient in that region. Since we shall continue to restrict the attention to the case $Ra_e = 0$, unless indicated otherwise, we shall drop the subscript i of Ra_i.

For the rigorous analysis of the onset problem in the limit of rapid rotation the dependence of the solution on the distance s from the axis must be considered which has been neglected in the application of the annulus model. It turns out that a finite difference exists between the results of the local analysis and the exact global analysis as was pointed out already by Soward (1977). Using a WKBJ approach with the double turning point method of Soward and Jones (1983), Yano (1992) has analyzed the asymptotic problem in a refined version of the rotating cylindrical annulus model. He assumes a finite gap and the same dependence on s of the small inclination of the convex conical end

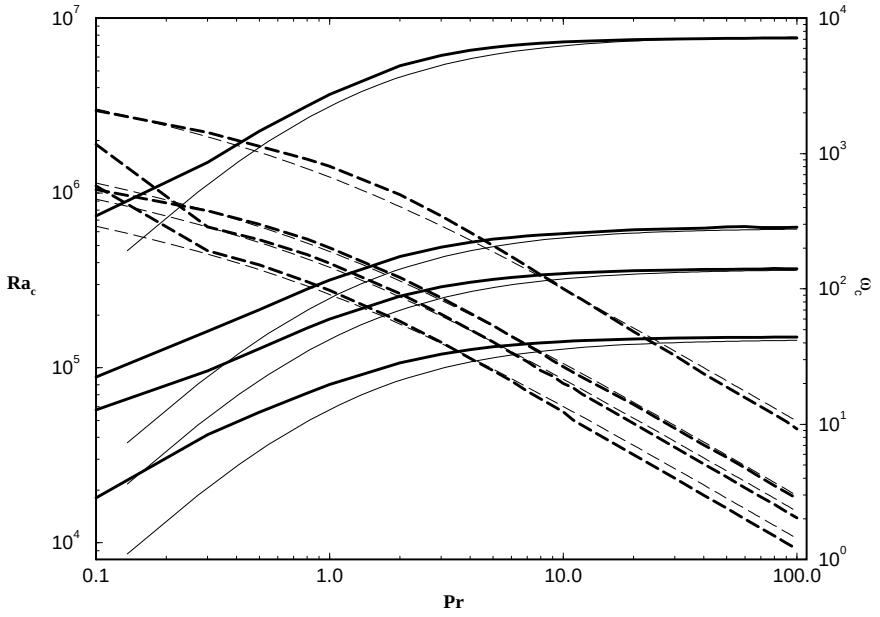

Figure 6: *Critical Rayleigh number Ra_{ic} (thick lines) and frequency ω_c (right ordinate, thick dashed lines) as a function of the Prandtl number Pr in the case $\eta = 0.4$ for the Coriolis numbers $\tau = 5 \cdot 10^3$, 10^4, $1.5 \cdot 10^4$ and 10^5. The thick solid line corresponds to expression (15a) and (15c).*

surfaces as in the case of the sphere. The component of gravity parallel to the axis of rotation is still neglected. These assumptions have been dropped by Jones et al. (2000), who attacked the full spherical problem. They find that their results agree surprisingly well with those of Yano (1992). The analytical findings have been confirmed through numerous numerical studies(Zhang and Busse, 1987; Zhang, 1991, 1992a; Ardes *et al.* 1997; Sun *et al.*, 1993) of which we show Fig. 7 as an example.This figure emphasizes the difference between the strongly spiralling nature of the convection columns at Prandtl numbers of the order unity or less and the more radially oriented columns at higher Prandtl numbers. This property is a result of the strong decrease of the frequency ω with increasing Pr.

The interest in convection in rotating spherical shells has motivated a number of laboratory investigations of the problem. The experiment of Hart et al. (1986) in which a spherically symmetric electric field acting on a dielectric insulating liquid is used to simulate gravity was carried out in space in order to avoid the interference from laboratory gravity. Less sophisticated experiments (Busse and Carrigan, 1976; Carrigan and Busse, 1983; Cardin and Olson, 1994;

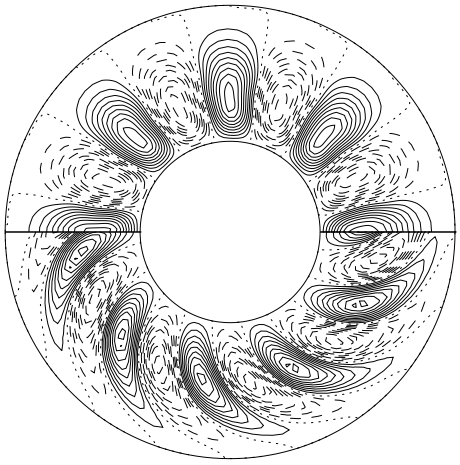

Figure 7: *Equatorial streamlines, $r\partial v/\partial\varphi$ = const., of convection columns in the cases $Pr = 10^5$, $\tau = 10^5$ and $Ra = 3 \cdot 10^6$ (upper half) and $Pr = 1$, $\tau = 10^4$ and $Ra = 2 \cdot 10^5$ (lower half).*

Cordero and Busse, 1992; Sumita and Olson, 2000) have used the centrifugal force with a cooled inner and a heated outer sphere to simulate the onset as well as the finite amplitude properties of convection. The main handicap of these experiments is the zonal flow generated as a thermal wind and the associated meridional circulation in the basic axisymmetric state (Cordero and Busse, 1992). But this handicap can be minimized through the use of high rotation rates and the observations correspond quite well to the theoretical expectations as shown by the example of Fig. 5.

5 Onset of Inertial Convection at Low Prandtl Numbers

Onset of instability in the form of inertial convection is well known from the case of a plane horizontal layer heated from below and rotating about a vertical axis. As has been discussed by Chandrasekhar (1961) convection in the form of modified inertial waves represents the preferred mode at the onset of instability for Prandtl numbers of the order 0.6 or less for sufficiently high values of the Coriolis number τ. A similar situation is found for convection in rotating spherical shells where Zhang and Busse (1987) identified equatorially attached modes of convection as modified inertial waves. This connection has

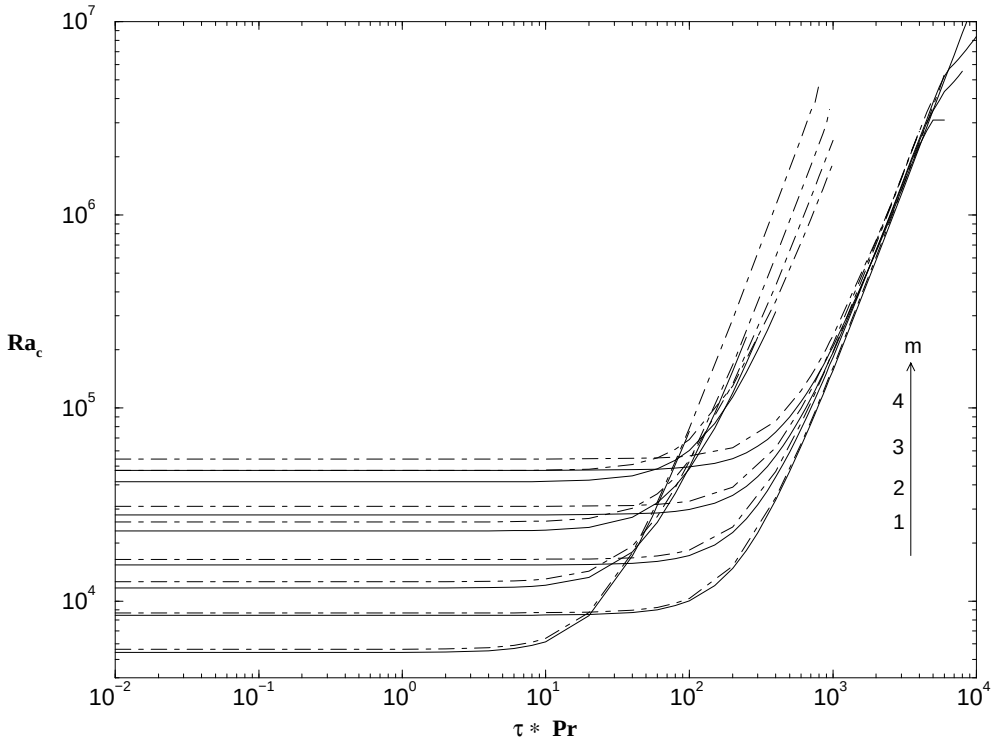

Figure 8: *The critical Rayleigh number Ra_c (solid lines) for the onset of the inertial convection as a function of τPr for various wavenumbers m. The dash-dotted lines correspond to the analytical expressions derived in Busse and Simitev (2004). For each m there are two modes corresponding to the two signs of ω in expression (17b). The retrograde mode corresponding to the positive sign is preferred at lower values of τPr. But it turns up before the prograde mode which thus is preferred for larger values of τPr.*

motivated Zhang (1994, 1995) to develop a perturbation approach for analytical description of the equatorially attached convection. Recently this approach has been extended and simplified by Busse and Simitev (2004). Here we shall just present a short introduction to the subject.

It is obvious from equations (11) even in their linearized versions that solutions for which the $r-$ and $\theta-$dependences separate are not admissible in general. Nevertheless for some parameter regimes simple, physically realistic solutions of the linearized version of Eqs. (11) together with conditions (13)

can be obtained through the separation ansatz

$$\begin{aligned} v &= P_m^m(\cos\theta)\exp\{im\varphi + i\omega t\}f(r), \\ w &= P_{m+1}^m(\cos\theta)\exp\{im\varphi + i\omega t\}g(r), \\ \Theta &= P_m^m(\cos\theta)\exp\{im\varphi + i\omega t\}h(r). \end{aligned} \tag{16}$$

Solutions of this form satisfy Eqs. (11) after the right hand sides have been dropped when the term proportional to P_{m+2}^m in the expression for Qw can be neglected. This term vanishes exactly in the limit of small Pr and high τ when the convection assumes the form of an inertial wave with the property

$$f(r) = \left(\frac{r}{r_o}\right)^m - \left(\frac{r}{r_o}\right)^{m+2},$$

$$g(r) = \frac{2im(m+2)(r/r_0)^{m+1}}{(2m+1)(\omega(m^2+3m+2)-m)r_o}, \tag{17a}$$

$$\omega = \frac{\tau}{m+2}(1 \pm (1+m(m+2)(2m+3)^{-1})^{\frac{1}{2}}). \tag{17b}$$

Since this solution does not satisfy all the boundary conditions (13), weak Ekman layers must be added and finite critical Rayleigh numbers for onset have thus been obtained (Zhang, 1994). Results for the Rayleigh number for different values of the azimuthal wavenumber m are shown in figure 8. According to these results the mode with $m = 1$ is always preferred in the case $\eta = 0$ if $Prtau$ is sufficiently low (Busse and Simitev, 2004). As $Prtau$ increases transition occurs to the mode propagating in the prograde direction. Besides the equatorially wall attached mode, convection can be described approximately in the form (16) if τ is less than 10^3 (see Ardes et al., 1997) or if the thin shell limit $\eta \to 1$ is approached (Busse, 1970b,1973).

6 Evolution of Convection Columns at Moderate Prandtl Numbers

In general the onset of convection in rotating fluid spheres occurs supercritically. As long as the convection assumes the form of shape preserving travelling thermal Rossby waves as described by linear theory, its azimuthally averaged properties are time independent. In fact, as seen from a frame of reference drifting together with the convection columns the entire pattern is steady. A differential rotation is generated through the action of the Reynolds stress as explained in section 2. The latter is caused by the spiralling cross section of

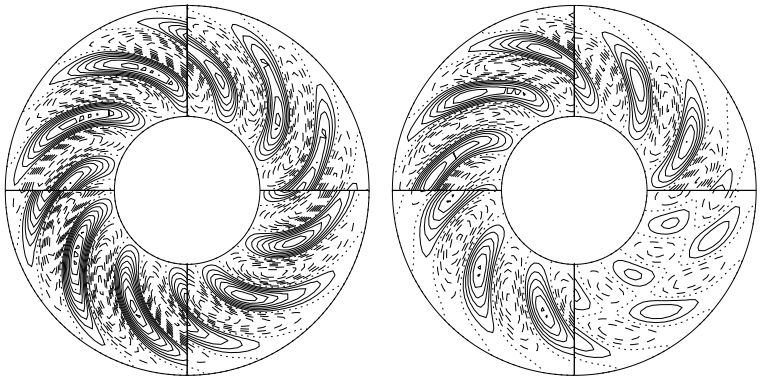

Figure 9: *Time periodic vacillations of convection at* $Ra = 2.8 \cdot 10^5$ *(left side) and* $Ra = 3 \cdot 10^5$ *(right side) for* $\tau = 10^4$, $Pr = 1$ *The streamlines,* $r\partial v/\partial\varphi = const.$ *are shown in one quarter of the equatorial plane. The four quarters are equidistant in time (with* $\Delta t = 0.015$ ($\Delta t = 0.024$) *in the left (right) case in the clockwise sense such that approximately a full period is covered by the circles.*

the columns which persists as a dominant feature at moderate Prandtl numbers far into the turbulent regime. The plots of the streamlines $r\frac{\partial v}{\partial \phi} = \text{const.}$ in the equatorial plane shown in any of the quarter circles of figure 9 give a good impression of the spiralling nature of the columns.

A true time dependence of convection develops in the form of vacillations after a subsequent bifurcation. First the transition to amplitude vacillations occurs in which case just the amplitude of convection varies periodically in time as exhibited in the left plot of figure 9. At a somewhat higher Rayleigh number shape vacillations become noticeable which are characterized by periodic changes in the structure of the columns as shown in the right plot of figure 9. The outer part of the columns is stretched out, breaks off and decays. The tendency towards breakup is caused by the fact that the local frequency of propagation varies with distance from the axis according to expression (15c) after θ_m has been replaced by the local colatitude θ.

The two types of vacillations also differ significantly in their frequencies of oscillation. This is evident from the time records of the energy densities of convection which have been plotted in figure 10. This figure gives an overview of the evolution of time dependence in the interval $2.8 \cdot 10^5 \leq Ra \leq 10^6$. The

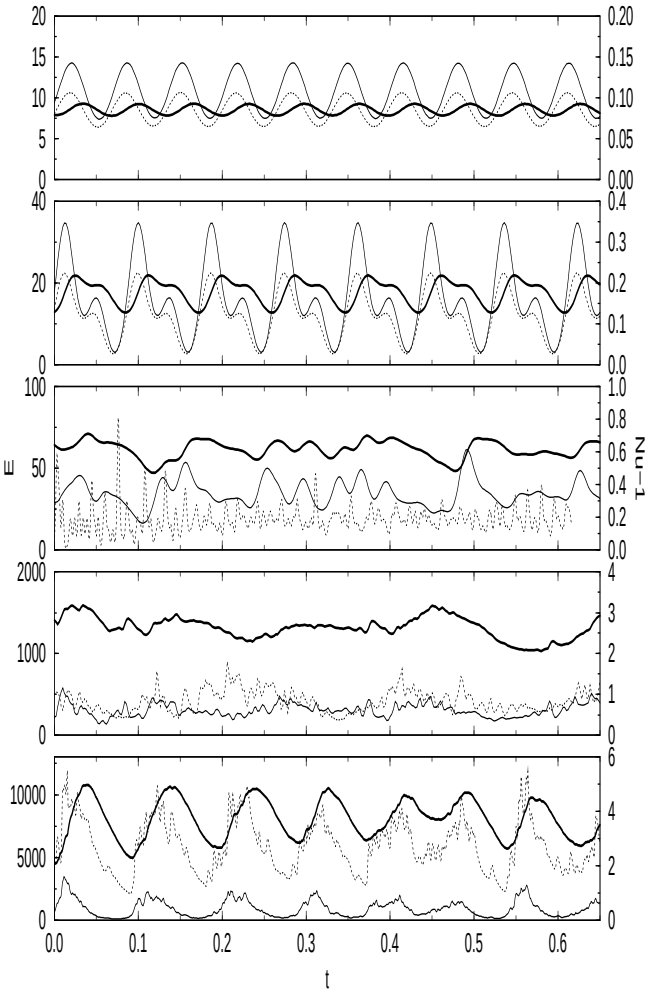

Figure 10: *Time series of energy densities E_t^m (thick solid lines), E_t^f (thin solid lines) and Nusselt number (dotted lines, right ordinate) are plotted for $Pr = 1$, $\tau = 10^4$, and $Ra = 2.8 \cdot 10^5$, $3 \cdot 10^5$, $3.5 \cdot 10^5$, $7 \cdot 10^5$ and $12 \cdot 10^5$ (from top to bottom). E_p^m and E_p^f have not been plotted. E_p^m is several orders of magnitude smaller than the other energies and E_p^f always approaches closely $0.4 \cdot E_t^f$.*

various components of the energy densities are defined by

$$E_p^m = \frac{1}{2}\langle \mid \nabla \times (\nabla \bar{v} \times \boldsymbol{r}) \mid^2 \rangle, \quad E_t^m = \frac{1}{2}\langle \mid \nabla \bar{w} \times \boldsymbol{r} \mid^2 \rangle \tag{18a}$$

$$E_p^f = \frac{1}{2}\langle \mid \nabla \times (\nabla \check{v} \times \boldsymbol{r}) \mid^2 \rangle, \quad E_t^f = \frac{1}{2}\langle \mid \nabla \check{w} \times \boldsymbol{r} \mid^2 \rangle \tag{18b}$$

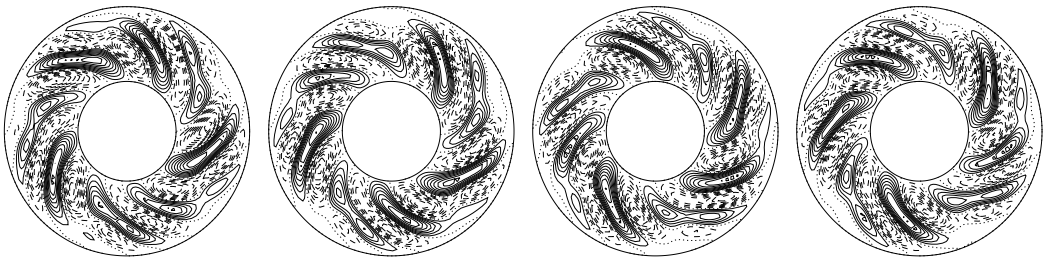

Figure 11: *Modulated shape vacillations of convection for* $Ra = 2.9 \cdot 10^5$, $\tau = 10^4$, $Pr = 1$. *The plots show streamlines,* $r\frac{\partial v}{\partial \phi} = const.$, *in the equatorial plane and are equidistant in time with* $\Delta t = 0.04$ *so that approximately a full period is covered.*

Figure 12: *Energy densities* E_t^m *(solid line),* E_p^m *(thin dashed line, multiplied by the factor 100),* E_t^f *(short dash - long dash line),* E_p^f *(thick dashed line) and the Nusselt number* Nu *(dotted line, right ordinate) are plotted as function of* $Ra - Ra_c$ *in the case* $\tau = 10^4$, $Pr = 1$. $Ra_c = 1.9 \cdot 10^5$ *has been used corresponding to* $m = 10$

where $\bar{v}$ refers to the azimuthally averaged component of v and $\check{v}$ is given by $\check{v} = v - \bar{v}$.

With a further increase of the Rayleigh number spatial modulations of the shape vacillations occur as shown in figure 11. These modulations often correspond to a doubling of the azimuthal period but soon contributions with the azimuthal wavenumber $m = 1$ arise as shown in figure 11. The pattern in this particular case is still periodic if appropriately sifted in azimuth. But as further modulations enter convection becomes quasiperiodic and with in-

creasing Ra a chaotic state is reached. We refer to the recent paper of Simitev and Busse (2003) which includes some movies to demonstrate the time dependence of convection. Figure 10 also demonstrates the diminishing fraction of the total kinetic energy that is associated with the poloidal component of motion which carries the convective heat transport. The differential rotation in particular increases much faster with Ra than the amplitude of convection since the Reynolds stress is proportional to the square of the latter. While this is already evident from the sequence of plots in figure 10 it is even more obvious from figure 12. Here it can also be seen that the onset of vacillations and aperiodic time dependence tends to increase the heat transport as indicated by the Nusselt number in contrast to the situation in a planar convection layer with the same Prandtl number (Clever and Busse, 1987). In the latter case the mismatch is absent between the structure of the convection flow and the configuration of the boundary which inhibits the heat transport in rotating spherical fluid shells. The time varying shift in the radial position of the convection columns thus promotes the heat transport.

Surprisingly the spatio-temporal randomness of convection columns does not just increase at larger values of Ra, but instead new coherent structures evolve (Grote and Busse, 2001). First there is localized convection as shown in Fig. 13. The differential rotation has become so strong that its shearing action inhibits convection in most parts of the spherical fluid shell as is evident from the figure. Only in a certain region of longitude is convection strong enough to overcome the shearing action of differential rotation. In the "quiet"zone the basic temperature profile recovers towards the purely conducting state and thus provides the buoyancy in the interior of the shell which sustains the localized convection as it is recirculated into the "active" zone by the differential rotation.

After a further amplification of the differential rotation with increasing Ra the local intensification of convection no longer suffices to overcome the shearing action of the zonal flow. Instead of a spatial separation between "active" and "quiet" zones the system chooses a separation in time which manifests itself in the relaxation oscillations seen in the lowermost plot of Fig. 10. The fluctuating component of motion is still rather turbulent in the case of the relaxation oscillation as demonstrated in Figs. 14 and 15. When the differential rotation has decayed sufficiently in the near absence of Reynolds stresses generated by convection, a sudden burst of convection activity occurs leading to a sharp peak in the heat transport. But since the Reynolds stress grows just as suddenly as the kinetic energy of convection, the growth of the differential rotation occurs with only a slight delay. The shearing off of the

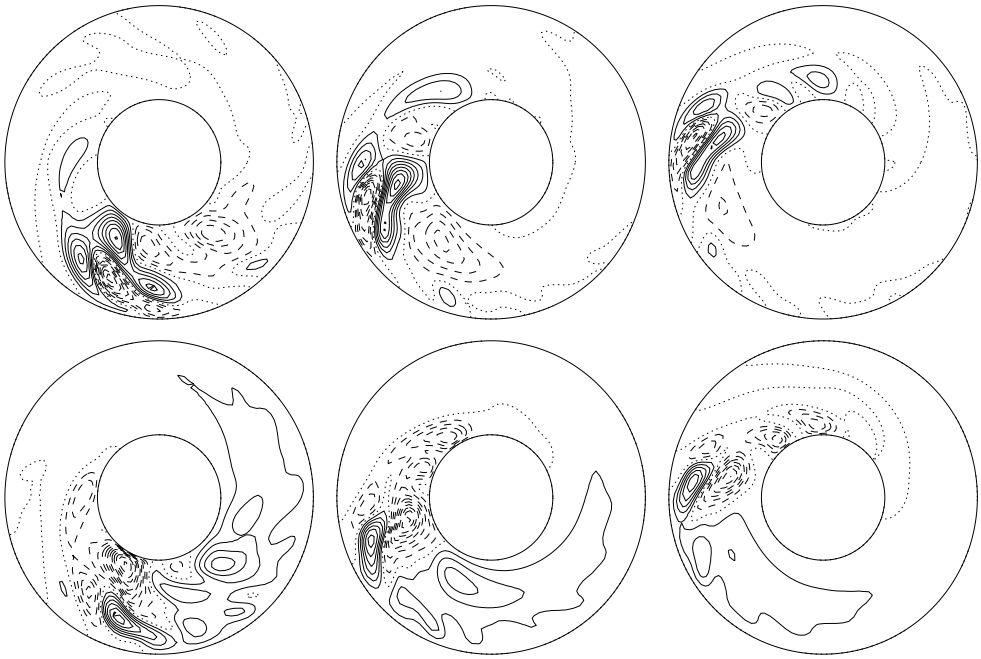

Figure 13: *Localized convection for* $Ra = 7 \cdot 10^5, \tau = 1.5 \cdot 10^4, Pr = 0.5$ *The streamlines,* $r\partial v/\partial\varphi = const.$ *(first row) and the isotherms,* $\Theta = const.$ *(second row), are shown in the equatorial plane for equidistant times (from left to right) with* $\Delta t = 0.03$*.*

convection columns then leads to their decay almost as quickly as they had set in. The relaxation oscillations occur over a wide region in the parameter space for high Rayleigh and Coriolis numbers and for Prandtl numbers of the order unity or less. Since it is mainly determined by the viscous decay of the differential rotation, the period of the relaxation oscillation does not vary much with these parameters. For the case of $\eta = 0.4$ which has been used for almost all numerical simulations a period of about 0.1 is usually found.

7 Finite Amplitude Convection at Higher Prandtl Numbers

The transitions from drifting convection columns to vacillating convection and modulated vacillating convection do not change much as as the Prandtl number tends to high values (Zhang, 1992b). But as Pr increases the influence of the

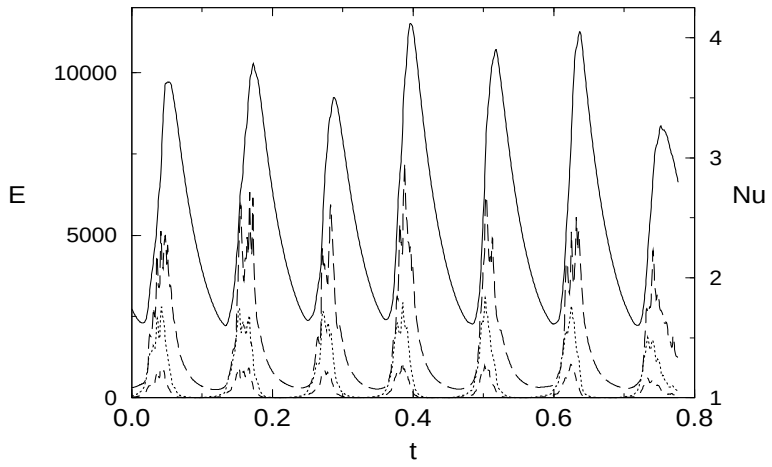

Figure 14: *Relaxation oscillation of turbulent convection in the case* $Ra = 10^6$, $\tau = 1.5 \cdot 10^4$, $Pr = 0.5$. *Energy densities* $\bar{E}_t$ *(solid line),* $\check{E}_t$ *(dotted line),* $\check{E}_p$ *(short dashed line) and the Nusselt number (long dashed line, right ordinate) are shown as functions of time* t.

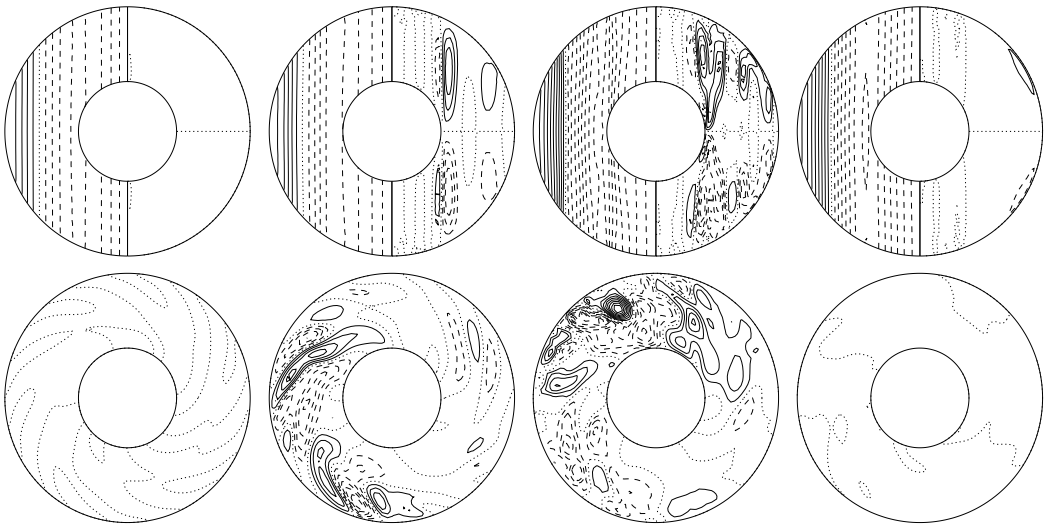

Figure 15: *Sequence of plots starting at* $t = 0.12015$ *and equidistant in time* ($\Delta t = 0.016$) *for the same case as in Fig. 14. Lines of constant* $\bar{u_\varphi}$ *and mean temperature perturbation,* $\bar{\Theta} = const.$ *in the meridional plane, are shown in the left and right halves, respectively, of the first row. The second row show streamlines,* $r\partial v/\partial\varphi = const.$, *in the equatorial plane.*

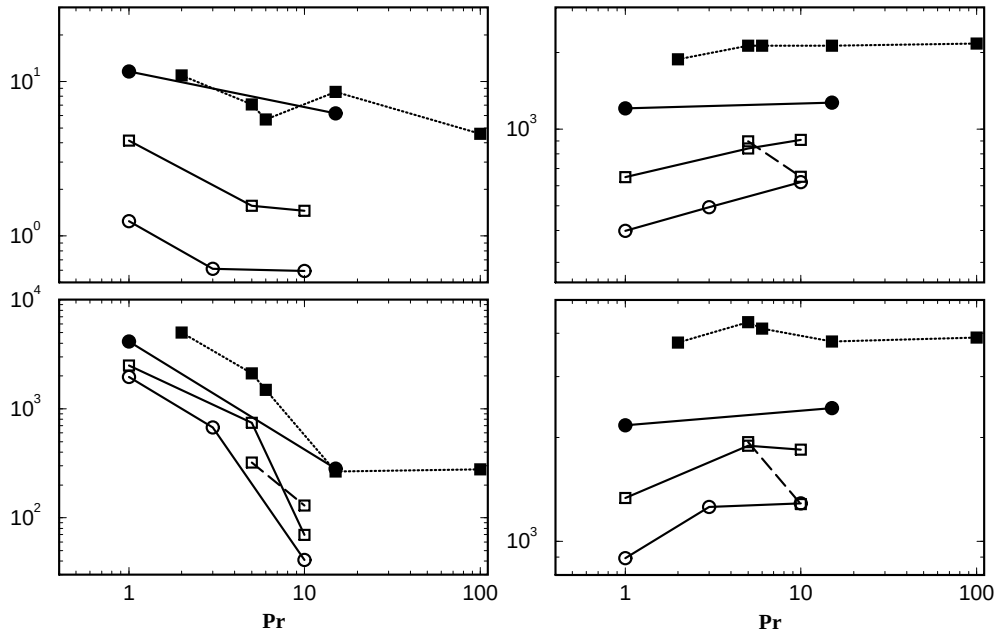

Figure 16: *Kinetic energy densities E_p^m (upper left panel), E_p^f (upper right panel), E_t^m (lower left panel) and E_t^f (lower right panel) all multiplied by Pr^2 as a function of the Prandtl number Pr in the case $\tau = 5 \cdot 10^3$. The values of the Rayleigh number $R = 5 \cdot 10^5$, $6 \cdot 10^5$, $8 \cdot 10^5$, 10^6 are denoted by empty circles and squares and full circles and squares, respectively.*

differential rotation which dominates the evolution of the convection columns for Prandtl numbers of the order unity and below diminishes rapidly. The feedback process exhibited most clearly by the mean flow instability discussed in section 2 ceases to operate at Prandtl numbers of the order 10. Above this value of Pr the properties of convection become nearly independent of Pr when the thermal time scale instead of the viscous one is used. This property which is familiar from Rayleigh-Bènard convection in plane layers heated from below holds rather generally in convection systems. For this reason we have plotted in figure 16 energy densities as defined by expressions (18), but multiplied by the factor Pr^2 in order to demonstrate the tendency towards independence of Pr. It should be noted that most of values used in this figure have been obtained from dynamo computations. But the action of the Lorentz force is rather weak and hardly affects the Prandtl number dependence of convection. Only the lower left plot for the energy densities of the differential rotation shows the expected strong decay with increasing Pr. These energy densities do not

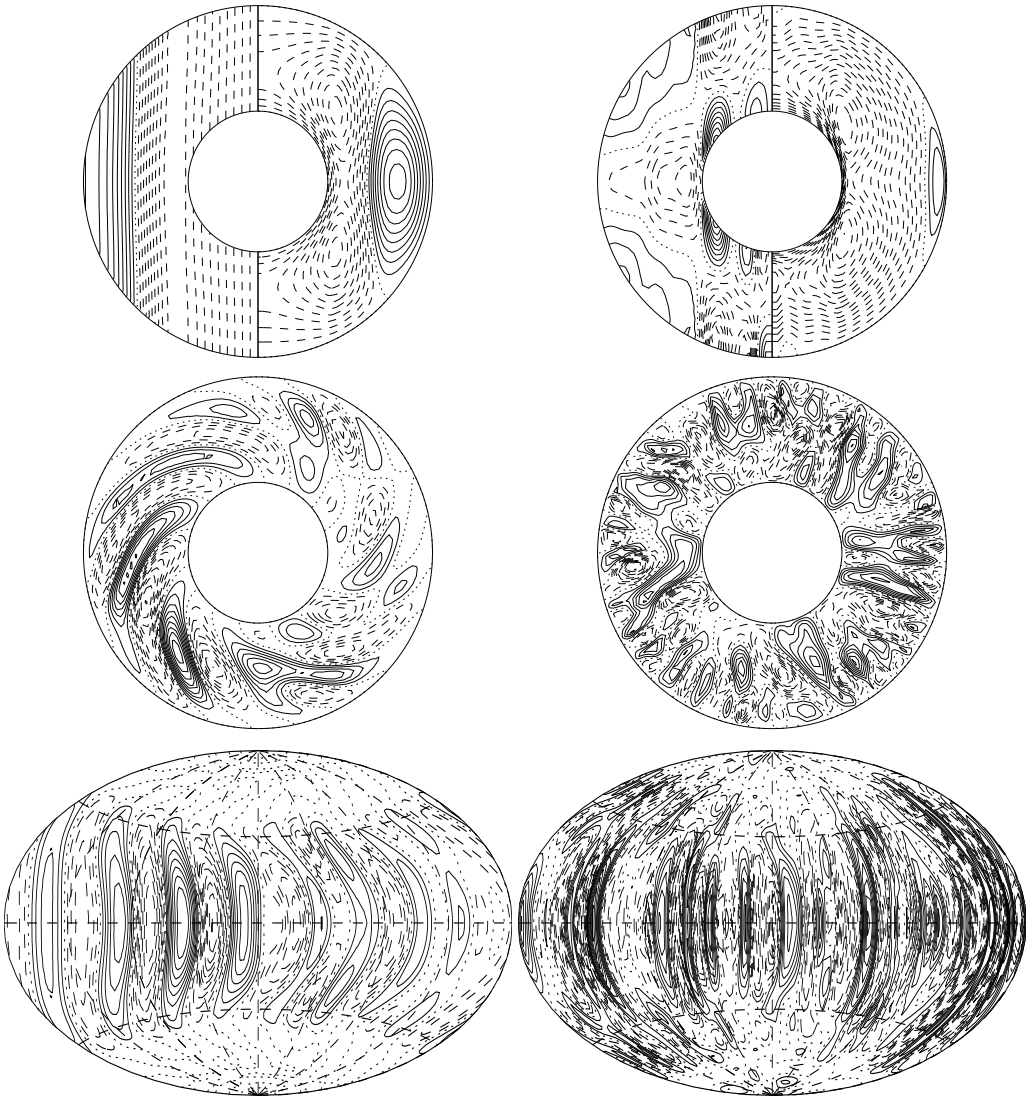

Figure 17: *Convection in rotating spherical fluid shells in the cases* $\tau = 10^4$, $Ra = 4 \cdot 10^5$, $Pr = 1$ *(left column) and* $\tau = 5 \cdot 10^3$, $Ra = 8 \cdot 10^5$, $Pr = 20$ *(right column). Lines of constant mean azimuthal velocity* $\bar{u}_\varphi$ *are shown in the left halves of the upper circles and isotherms of* $\bar{\Theta}$ *are shown in the right halves. The plots of the middle row show streamlines,* $r\partial v/\partial\varphi = const.$*, in the equatorial plane. The lowermost plots indicate lines of constant* u_r *in the middle spherical surface,* $r = r_i + 0.5$.

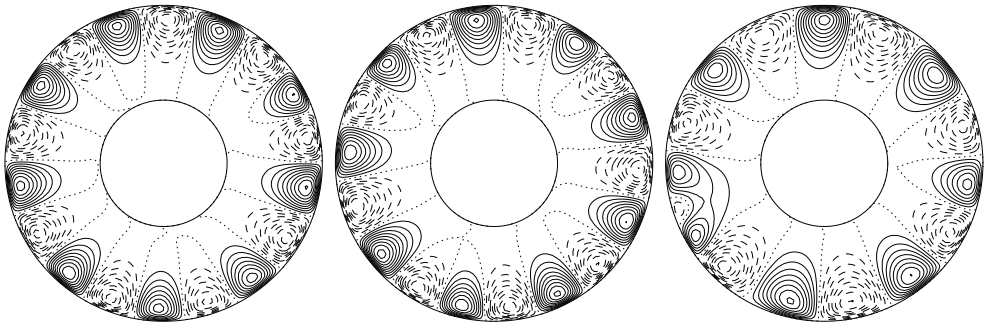

Figure 18: *Streamlines* $r\frac{\partial v}{\partial \phi} = const.$ *in the equatorial plane for the case* $Pr = 0.025$, $\tau = 10^5$ *with* $Ra = 3.2 \cdot 10^5$, $3.4 \cdot 10^5$, $4 \cdot 10^5$ *(from left to right).*

decay to zero for $Pr \to 0$, however. The thermal wind relationship obtained from the azimuthal average of the ϕ-component of the curl of equation (10a)

$$\tau \mathbf{k} \cdot \nabla \bar{u}_\phi = \partial_\theta \bar{\Theta} \tag{19}$$

continues to require a finite field $\bar{u}_\phi$ in the limit of high Pr. The right hand side is finite because the azimuthally averaged temperature field $\bar{\Theta}$ deviates strongly from spherical symmetry as long as the influence of rotation is significant.

The typical differences between convection at Prandtl numbers of the order unity and higher values are exhibited in figure 17 where typical results obtained for $Pr = 1$ and $Pr = 20$ are compared at similar values of Ra and τ. The approximate validity of the thermal wind relationship (19) can be noticed from a comparison of the plots of $\bar{u}_\phi$ and of $\bar{\Theta}$ in the case $Pr = 20$. The convection columns retain their alignment with the axis of rotation with increasing Pr, but the spiralling nature of their radial orientation disappears.

8 Finite Amplitude Inertial Convection

For an analysis of nonlinear properties of equatorially attached convection we focus on the case $Pr = 0.025$ with $\tau = 10^5$. The critical Rayleigh number for this case is $Ra_c = 28300$ corresponding to $m = 10$. As Ra is increased beyond the critical value other values of m from 7 to 12 can be realized, but $m = 10$ and lower values are usually preferred. An asymptotic perfectly periodic solution with $m = 10$ or $m = 9$ can be found only for Rayleigh numbers close to the critical value when computations are started from arbitrary initial conditions. On the other hand, perfect periodic patterns appear to be stable

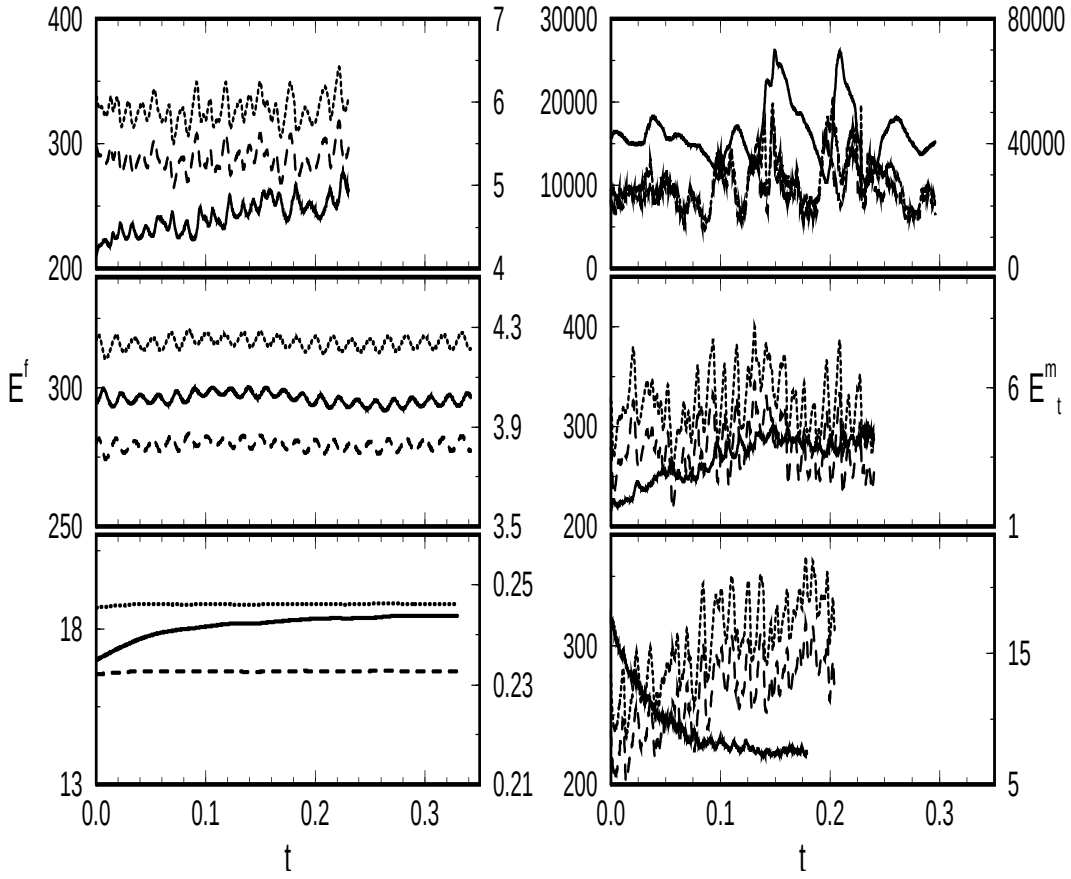

Figure 19: *Time series of energy densities of convection in the case* $Pr = 0.025$, $\tau = 10^5$, *for* $Ra = 3.1 \cdot 10^5$, $3.2 \cdot 10^5$, $3.4 \cdot 10^5$, *(from bottom to top, left side) and* $3.8 \cdot 10^5$, $4 \cdot 10^5$, $8 \cdot 10^5$ *(from bottom to top, right side). The solid, dotted and dashed lines correspond to* E_t^m, E_t^f, E_p^f , *respectively.* E_t^m *is measured on the right ordinate.*

with respect to small disturbances over a more extended regime of supercritical Rayleigh numbers. Distinct transitions like the transition to amplitude vacillations and to structure vacillations do not seem to exist for equatorially attached convection. Instead modulated patterns are typically already observed when Ra exceeds the critical value by 10% as can be seen in the plots of figure 18. These modulations are basically caused by the superposition of several modes with neighboring values of the azimuthal wavenumber m which appear to propagate nearly independently. For example, the period of $1.68 \cdot 10^{-2}$ visible in the energy densities shown in figure 19 in the case

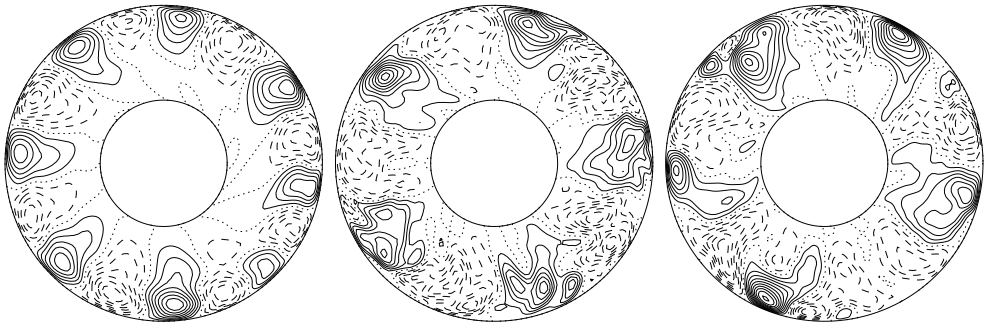

Figure 20: *Streamlines* $r\frac{\partial v}{\partial \phi} = const.$ *in the equatorial plane for the case* $Pr = 0.025$, $\tau = 10^5$ *with* $Ra = 6 \cdot 10^5$, $8 \cdot 10^5$, 10^6 *(from left to right).*

$Ra = 3.2 \cdot 10^5$ is just about half the difference of $3.34 \cdot 10^{-2}$ between the periods of the modes $m = 8$ and $m = 9$ according the inertial wave dispersion relation (17b) for prograde modes. This property must be expected if a small component with $m = 8$ participates in the pattern shown in figure 18 which is dominated by the $(m = 9)$-component. The time series of energy densities shown in figure 19 indicate that usually more than two modes contribute to the dynamics of the pattern with the exception of the case just discussed since the time dependence is not periodic as in the case when only two modes interact. The computations of the time series require a high spatial resolution together with a small time step. The time spans indicated in figure 19 are sufficient for reaching a statistically steady state of the fluctuating components of motion since these equilibrate on the fast thermal time scale of the order Pr^{-1}. Only close to Ra_c the adjustment process takes longer as can be seen in the case $Ra = 3.1 \cdot 10^5$ where a $(m = 10)$-pattern approaches its equilibrium state. The pattern corresponding to the other cases of figure 19 are shown in figures 18, and 20. The differential rotation represented by E_t^m relaxes on the viscous time scale and therefore takes a long time to reach its asymptotic regime in the examples shown in figure 19. But the differential rotation is quite weak such that it has a negligible effect on the other components of motion except in the case of the highest Rayleigh number of figure 19. Even smaller is the axisymmetric part of the poloidal component of motion which is not shown in the plots of figure 19. At higher Rayleigh numbers the convection eddies spread farther into the interior and in some cases become detached from the equator as can be seen in the plots of figure 20. In this way the convection eddies contribute to the heat transport from the inner boundary. But at the

same time they acquire the properties of the convection columns which are characteristic for convection at higher Prandtl numbers. Accordingly the differential rotation is steeply increased at $Ra = 10^6$ and a tendency towards relaxation oscillation can be noticed in the upper right time series of figure 19. For additional details on low Prandtl number spherical convection we refer to Simitev and Busse (2003).

References

Ardes, M., Busse, F.H., and Wicht, J., Thermal Convection in Rotating Spherical Shells, *Phys. Earth Planet. Int.* **99**, 55-67, (1997)

Bell, P.I., and Soward, A.M., The influence of surface topography on rotating convection, *J. Fluid Mech.* **313**, 147-180, (1996)

Bisshopp, F.E. and Niiler, P.P., Onset of convection in a rapidly rotating fluid sphere, *J. Fluid Mech.* **23**, 459-469, (1965)

Brummell, N.H., and Hart, J.E., High Rayleigh number β-convection, *Geophys. Astrophys. Fluid Dyn.* **68**, 133-150, (1993)

Busse, F.H., Thermal instabilities in rapidly rotating systems, *J. Fluid Mech.* **44**, 441-460, (1970a)

Busse, F.H., Differential rotation in stellar convection zones, *Astrophys. J.* **159**, 629-639, (1970b)

Busse, F.H., Differential Rotation in Stellar Convection Zones II, *Astron. & Astrophys.* **28**, 27-37, (1973)

Busse, F.H., On the problem of stellar rotation, *Astrophys. J.*, **259**, 759-766, (1982)

Busse, F.H., and Carrigan, C.R., Convection induced by centrifugal buoyancy, *J. Fluid Mech.* **62**, 579-592, (1974)

Busse, F.H., and Carrigan, C.R., Laboratory simulation of thermal convection in rotating planets and stars, *SCIENCE* **191**, 81-83, (1976)

Busse, F.H., and Hood, L.L., Differential rotation driven by convection in a rotating annulus, *Geophys. Astrophys. Fluid Dyn.* **21**, 59-74, (1982)

Busse, F.H., and Simitev, R., Inertial convection in rotating fluid spheres, submitted to *Phys. Fluids*, (2004)

Cardin, P., and Olson, P., Chaotic thermal convection in a rapidly rotating spherical shell: consequences for flow in the outer core, *Phys. Earth Planet. Inter.* **82**, 235-259, (1994)

Carrigan, C.R., and Busse, F.H., An experimental and theoretical investigation of the onset of convection in rotating spherical shells, *J. Fluid Mech.* **126**, 287-305, (1983)

Chandrasekhar, S., "Hydrodynamic and Hydromagnetic Stability", Oxford: Clarendon Press (1961)

Chen, C. X., and Zhang, Keke, Nonlinear convection in a rotating Annulus with a finite gap, *Geophys. Astrophys. Fluid Dyn.* **96**, 519-518 (2002)

Clever, R.M., and Busse, F.H., Nonlinear oscillatory convection, *J. Fluid Mech.* **176**,403-417 (1987)

Cordero, S., and Busse, F.H., Experiments on convection in rotating hemispherical shell: Transition to quasi-periodic state, *Geophys. Res. Letts.* **19**, 733-736, (1992)

Geiger, G., and Busse, F.H., On the onset of thermal convection in slowly rotating fluid shells, *Geophys. Astrophys. Fluid Dyn.* **18**, 147-156 (1981)

Grote, E., and Busse, F.H., Dynamics of convection and dynamos in rotating spherical fluid shells, *Fluid Dyn. Res.* **28**, 349-368, (2001)

Hart, J.E., Glatzmaier, G.A., and Toomre, J., Space-laboratory and numerical simulations of thermal convection in a rotating hemispherical shell with radial gravity, *J. Fluid Mech.* **173**, 519-544, (1986)

Herrmann, J., and Busse, F.H., Convection in a Rotating Cylindrial Annulus. Part 4. Modulations and Transition to Chaos at Low Prandtl Numbers, *J. Fluid Mech.* **350**, 209-229, (1997)

Jones, C.A., Soward, A.M., and Mussa, A.I., The onset of thermal convection in a rapidly rotating sphere, *J. Fluid Mech.* **405**, 157-179, (2000)

Or, A.C., and Busse, F.H., Convection in a rotating cylindrical annulus. Part 2. Transitions to asymmetric and vacillating flow, *J. Fluid Mech.* **174**, 313-326, (1987)

Pino, D., Mercader, I., and Net, M., Thermal and inertial modes of convection in a rapidly rotating annulus, *Phys. Rev. E* **61**, 1507-1517, (2000)

Pino, D., Net, M., Sanchez, J., and Mercader, I.,Thermal Rossby waves in a rotating annulus, *Phys. Rev. E* **63**, 056312, (2001)

Roberts, P.H., On the thermal instability of a highly rotating fluid sphere, *Astrophys. J.* **141**, 240, (1965)

Roberts, P.H., On the thermal instability of a rotating-fluid sphere containing heat sources, *Phil. Trans. Roy. Soc. London* **A 263**, 93-117, (1968)

Schnaubelt, M., and Busse, F.H., Convection in a rotating cylindrical annulus. Part 3. Vacillating and spatially modulated flow, *J. Fluid Mech.* **245**, 155-173, (1992)

Soward, A.M., On the finite amplitude thermal instability in a rapidly rotating fluid sphere, *Geophys. Astrophys. Fluid Dyn.* **9**, 19-74, (1977)

Simitev, R., and Busse F.H., Patterns of convection in rotating spherical shells, *New J. Phys.* **5**, 1.1-1.20, (2003)

Soward, A.M., and Jones, C.A., The linear stability of the flow in the narrow gap

between two concentric rotating spheres, *Q. J. Mech. Appl. Maths.* **36**, 19-42, (1983)

Sumita, I., and Olson, P., Laboratory experiments on high Rayleigh number thermal convection in a rapidly rotating spherical shell, *Phys. Earth Planet. Inter.* **117**, 153-170, (2000)

Sun, Z.-P., Schubert, G., and Glatzmaier, G.A., Transitions to chaotic thermal convection in a rapidly rotating spherical fluid shell, *Geophys. Astrophys. Fluid Dyn.* **69**, 95-131, (1993)

Tilgner, A., and Busse, F.H., Finite amplitude convection in rotating spherical fluid shells, *J. Fluid Mech.* **332**, 359-376, (1997)

Westerburg, M., and Busse, F.H., Centrifugally driven convection in the rotating cylyndrical annulus with modulated boundaries, *nonlin. Processes in Geophys.* **10**, 275-280, (2003)

Yano, J.-I., Asymptotic theory of thermal convection in rapidly rotating system, *J. Fluid Mech.* **243**, 103-131, (1992)

Zhang, K.-K., and Busse, F.H., On the onset of convection in rotating spherical shells, *Geophys. Astrophys. Fluid Dyn.* **39**, 119-147, (1987)

Zhang, K., Convection in a rapidly rotating spherical fluid shell at infinite Prandtl number: steadily drifting rolls, *Phys. Earth Planet. Int.* **68**, 156-169, (1991)

Zhang, K., Spiraling columnar convection in rapidly rotating spherical fluid shells, *J. Fluid Mech.* **236**, 535-556, (1992a)

Zhang, K., Convection in a rapidly rotating spherical shell at infinite Prandtl number: transition to vacillating flows, *Phys. Earth. Plan Int.* **72**, 236-248, (1992b)

Zhang, K., On coupling between the Poincaré equation and the heat equation, *J. Fluid Mech.* **268**, 211-229, (1994)